JPEDAV (2007) 28:90–100
DOI: 10.1007/s11669-006-9014-5
1547-7037 ©ASM International

Thermodynamic Calculations and Phase Stabilities in the Y-Si-C-O System

Damian M. Cupid and Hans J. Seifert

(Submitted October 30, 2006)

A thermodynamic computer dataset for the Y-Si-C-O system was used for calculations of multicomponent, multiphase reactions. The phase reactions of yttrium silicate coatings for the oxidation protection of C/SiC-based composites were analyzed. They were simulated as a function of the temperature and other environmental conditions. To illustrate the high temperature behavior of the coatings, isothermal sections, isopleths, pseudo-binary and -ternary diagrams, phase fraction diagrams, volatility diagrams and potential phase diagrams are presented. Additionally to the thermodynamic aspects, mass balance criteria were taken into account for the analysis of the active/passive oxidation in the coating system.

Keywords CALPHAD, heat shields, Y-Si-C-O system, yttrium silicate coatings

1. Introduction

The Y-Si-C-O system is a key system for the understanding of a manifold of engineering materials composed of SiC and yttrium silicates, respectively. For example, the system is of major interest for the understanding of the liquid phase sintering of SiC ceramics using oxide additives such as Y_2O_3.[1] In addition, phase reactions in this quaternary system have to be understood to analyze the compatibility and reactions of protective yttrium silicate coatings on carbon fiber reinforced carbon-based composite engineering materials. The yttrium silicate Y_2SiO_5 was introduced by Ogura et al.[2] as a promising candidate material for the oxidation protection of such materials (e.g., carbon/carbon (C/C), carbon/silicon carbide (C/SiC, C/C-SiC)). For high temperature structural applications, a two-layer coating system consisting of yttrium silicates deposited on a Chemical-Vapor-Deposition-SiC (CVD-SiC) bond coating can be used. This design has the potential for applications as a protective multilayer coating system in gas turbines and reusable space shuttle systems. Various methods such as slip casting,[3–5] atmospheric plasma spraying (APS),[2,6,7] low pressure plasma spraying (LPPS),[8,9] and the sol-gel process[10,11] were tested to deposit yttrium silicate coatings on SiC pre-coated composites. The different fabrication methods result in significantly different coating compositions and microstructures. The coating may consist of only Y_2SiO_5 (X_1 or X_2 modification) or mixtures of this compound with $Y_2Si_2O_7$ (α-, β-, γ-, δ-modifications). Additionally, excess SiO_2 or Y_2O_3 have to be taken into account. To evaluate the applications of these different coating compositions, it is important to analyze their high temperature phase reactions. The methods of computational thermodynamics can support an experimental analysis.

A thermodynamic dataset for the quaternary Y-Si-C-O system was developed and applied to the evaluation of the phase reactions of the two-layer coatings on a C/C-SiC substrate. Plasma wind tunnel experiments show that dense LPPS-derived $Y_2SiO_5/Y_2Si_2O_7$ coatings provide a very good oxidation protection for a CVD-SiC coating and the C/C-SiC substrate up to temperatures of 1923 K. At higher temperatures ($T > 1650$°C) blister formation can be detected.[9,12] Additionally, large pores occur within the yttrium silicate coating. Thermodynamic calculations show that gas phase formation from the coating system or substrate reactions causes this effect. A significant CO gas pressure development for temperatures higher than 1650 °C was detected.[12] The present work evaluates the reactions and gas phase development for various yttrium silicate coatings containing Y_2O_3 and SiO_2, respectively.

2. Thermochemical Calculations

The CALPHAD (CALculation of PHAse Diagram) method was used to determine phase equilibria and phase reactions in multicomponent systems.[13] The unary data for the pure elements and the description for the gaseous species were taken from the SGTE substance database.[14] The thermodynamic descriptions for the binary systems Y-Si, Y-C, Si-C, and Y-O were derived by thermodynamic

This article was presented at the MultiComponent Alloy Thermodynamics Symposium sponsored by the Alloy Phase Committee of the joint EMPMD/SMD of The Minerals, Metals, and Materials Society (TMS), held in San Antonio, Texas, March 12–16, 2006, to honor the 2006 William Hume-Rothery Award recipient, Professor W. Alan Oates of the University of Salford, UK. The symposium was organized by Y. Austin Chang of the University of Wisconsin, Madison, WI, Patrice Turchi of the Lawrence Livermore National Laboratory, Livermore, CA, and Rainer Schmid-Fetzer of the Technische Universitat Clausthal, Clauthal-Zellerfeld, Germany.

Damian M. Cupid, and **Hans J. Seifert,** Department of Materials Science and Engineering, University of Florida, Gainesville, FL32611-6400, USA; Contact e-mail: seifert@ww.tu-freiberg.de

optimization[15,16] and the system Si-O was taken from literature.[17] Based on phase diagram data and measurements of enthalpy of formation and heat capacity for the solid phases, a thermodynamic assessment of the system Y_2O_3-SiO_2 was developed.[18] These descriptions were combined in one single thermodynamic database to calculate the phase equilibria in the quaternary Y-Si-C-O system. The database contains Gibbs free-energy data for the following phases: yttrium (α, β), silicon, graphite, Y_2O_3 (α, β), SiO_2 (quartz, tridymite, cristobalite), SiC (α, β), $Y_2Si_2O_7$ (α, β, γ, δ), Y_2SiO_5 (X_1, X_2), yttrium carbide (γ), Y_3C_4 (h, r), YC_2 and the yttrium silicides (Y_5Si_3, Y_5Si_4, YSi, Y_3Si_5 (h, r), YSi_2). Additionally, metallic and oxide liquid phases and the most important gas species (e.g., O_2, CO, CO_2, SiO) were taken into account. For the description of the liquid phase, the two-sublattice ionic liquid model was used. The phase reactions were calculated using the software BINGSS, BINFKT,[19] and THERMO-CALC.[20] Table 1 lists the descriptions for the Y_2O_3-SiO_2 and the Si-C systems including the gaseous species which were used for the calculations of the coating reactions.

The quaternary dataset enables calculation of all types of phase diagrams and thermodynamic functions in the quaternary system. The calculated isothermal sections of the ternary Y-Si-C-O subsystems for a temperature of 1650 °C are presented in Fig. 1. Similar calculations are possible at all temperatures of interest and provide important information on the complex phase equilibria. The calculated pseudo-binary Y_2O_3-SiO_2 phase diagram in the Y-Si-O subsystem is presented in Fig. 2.[18] There are two main yttrium silicate compounds in the Y_2O_3-SiO_2 system, the monosilicate (Y_2SiO_5) and the disilicate ($Y_2Si_2O_7$). Y_2SiO_5 has two polymorphs designated X_1 and X_2. $Y_2Si_2O_7$ has four modifications, designated α, β, γ, and δ in order of increasing temperature. Calculation results show that Y_2SiO_5 melts congruently at 1959 °C and $Y_2Si_2O_7$ melts incongruently at 1787 °C. The calculated binary Si-C phase diagram is presented in Fig. 3.[15] SiC exists in two modifications: cubic β-SiC and hexagonal α-SiC. No distinction was made between β-SiC and α-SiC in the thermodynamic modeling of SiC. SiC melts incongruently at 2823 °C to produce the Si-rich liquid and graphite. A degenerate eutectic point between Si-rich liquid, Si and SiC occurs at 1414 °C. Figure 4 shows the calculated 1650 °C isotherm for the pseudo-ternary SiO_2-Y_2O_3-SiC subsystem which is a section through the quaternary system. Three three-phase equilibria are shown: (a) SiC, SiO_2 (cristobalite), and $Y_2Si_2O_7$, (b) SiC, Y_2SiO_5 and $Y_2Si_2O_7$, and (c) SiC, Y_2O_3 and Y_2SiO_5. These equilibria represent possible coating systems based on yttrium silicates and (excess) SiO_2 and Y_2O_3, respectively. The phases are additionally in contact with SiC and carbon from the CVD-SiC coating and potentially the substrate itself.

3. Calculations of Chemical Compatibility

To investigate the stability of the SiC-Y_2SiO_5-$Y_2Si_2O_7$ phase field (Fig. 4), calculations were performed for a closed system. The influence of an increasing oxygen partial pressure on an initial mixture of one mole of SiC, 0.67 mole Y_2SiO_5 and 0.33 mole $Y_2Si_2O_7$ was simulated. Argon (Ar) was used as an inert gas in the closed system so that the software would generate a gas phase. Figure 5(a) shows the calculated phase fraction diagram resulting from the phase reactions at 1650 °C. The amounts of the input phases were chosen according to the typical phase fractions in the coatings. The oxygen partial pressure p_{O_2} is used as the abscissa. As shown elsewhere, in the absence of gaseous oxygen no reactions of the solid phases occur over extended temperature ranges.[12] Figure 5(a) shows that there is no reaction between the yttrium silicates and SiC up to a partial pressure of $p_{O_2} = 10^{-15.1}$ bar. At higher pressures, however, monosilicate reacts with SiC and oxygen to produce disilicate and gas phase (consisting of gaseous species SiO and CO). The decreasing amount of residual SiC corresponds to an active oxidation of SiC formally described by the reaction

$$SiC + O_2(g) = SiO(g) + CO(g) \quad \text{(Eq 1)}$$

Figure 5(b) shows the development of the equilibrium number of moles of major gas species in the atmosphere with p_{O_2} for the corresponding reactions. The lines AB and CD in Fig. 5(b) confirm that SiO(g) and CO(g) are produced in equal amounts during active oxidation of residual SiC. Up to p_{O_2} of $10^{-14.45}$ bar, SiC and SiO_2 are in equilibrium. Beyond this point, SiO_2 alone is stable. According to these equilibrium calculations, the active to passive transition for SiC occurs at a p_{O_2} of $10^{-14.45}$ bar which is much lower than that observed experimentally (~10^{-3} bar).[21–23] To take this observation into account, in a next approach, calculations for metastable conditions were performed by suspending the SiO_2 phase. The results are shown in Fig. 6(a) and (b). They indicate that active oxidation of SiC continues until it is completely consumed at a pressure of $p_{O_2} = 10^{-13.9}$ bar. Obviously these approaches of calculating stable and metastable equilibria cannot explain the experimental observations of SiC coatings surfaces or interfaces.

3.1 Active/Passive Oxidation of SiC

Heuer and Lou[24] referred to the work of Wagner[25] and showed that calculated volatility diagrams combined with mass-balance considerations can explain the active to passive transition for silicon carbide. In cases where reactions between the solid surface phases (e.g., SiC) and gaseous species (e.g., O_2) occur, such mass-balance constraints apply. The volatilization will create its own gaseous environment at the interface. The active oxidation of SiC is described by Eq 1. During the atmospheric re-entry of the space shuttle or in the gas turbine environment, oxygen molecules diffuse through a gaseous boundary layer toward the SiC surface, whereas CO and SiO diffuse through a gaseous boundary layer away from the SiC surface. If the rate-determining mechanism for the reaction is assumed to be the gaseous transport of oxygen to the SiC surface, then under steady-state conditions, the flux of oxygen impingement at the SiC surface

Table 1 Thermodynamic descriptions as used for the calculation of yttrium silicate coating reactions

O_2, gas

$G(Gas, O_2) =$
$298.14 - 1000 : -6961.74451 - 76,729.7484 \cdot T^{-1} - 51.0057202 - 22.2710136 \cdot T \cdot \ln T - 0.0101977469 \cdot T^2 + 1.32369208 \cdot 10^{-6} \cdot T^3$
$1000 - 3300 : -13,137.5203 + 525,809.556 \cdot T^{-1} + 25.3200332 - 33.627603 \cdot T \cdot \ln T - 0.00119159274 \cdot T^2 + 1.35611111 \cdot 10^{-8} \cdot T^3$
$3300 - 6000 : -27,973.4908 + 876,6421.4 \cdot T^{-1} + 62.5195726 - 37.9072074 \cdot T \cdot \ln T - 8.50483772 \cdot 10^{-4}2 + 2.14409777 \cdot 10^{-8} \cdot T^3$

CO, gas

$G\ (Gas, CO) =$
$298.14 - 800 : -118,162.172 - 55,604.1048^{-1} - 23.0733171 \cdot T - 25.8462416 \cdot T \cdot -0.00328155304 \cdot T^2 - 1.63612531 \cdot 10^{-7} \cdot T^3$
$800 - 2200 : -122211.067 + 541,480.728 \cdot T^{-1} + 7.7192763 - 29.9366037 \cdot T \cdot \ln T - 0.00270531164 \cdot T^2 + 1.75559245 \cdot 10^{-7} \cdot T^3$
$2200 - 6000 : -131,274.232 + 2,724,014.12 \cdot T^{-1} + 62.2289327 - 37.1759278 \cdot T \cdot \ln T - 1.02023702 \cdot 10^{-4}2 - 6.44914787 \cdot 10^{-10} \cdot T^3$

CO_2, gas

$G(Gas, CO_2) =$
$298.14 - 800 : -404,174.688 + 93,852.9776^{-1} - 15.6755321 \cdot T - 27.5390043 \cdot T \cdot \ln T - 0.0223193388 \cdot T^2 + 3.00075783 \cdot 10^{-6} \cdot T^3$
$800 - 1800 : -415,639.481 + 1,325,131.38 \cdot T^{-1} + 121.627014 - 47.9557528 \cdot T \cdot \ln T - 0.00577969392 \cdot T^2 + 4.24028177 \cdot 10^{-7} \cdot T^3$
$1800 - 4000 : -430,260.277 + 4,427,090.4 \cdot T^{-1} + 219.575601 - 61.1863976 \cdot T \cdot \ln T - 3.6174864 \cdot 10^{-4} \cdot T^2 + 2.80415864 \cdot 10^{-9} \cdot T^3$
$4000 - 6000 : -442,257.528 + 9,866,897.08 \cdot T^{-1} + 259.41716 - 66.0264488 \cdot T \cdot \ln T + 4.88768604 \cdot 10^{-4} \cdot T^2 - 2.47381789 \cdot 10^{-8} \cdot T^3$

SiO, gas

$G(Gas, SiO) =$
$298.14 - 800 : -107859.68 - 42908.8028^{-1} - 53.9139083 \cdot T - 22.5627221 \cdot T \cdot \ln T - 0.0125249295 \cdot T^2 + 2.05530632 \cdot 10^{-6} \cdot T^3$
$800 - 3400 : -115307.101 + 720030.836 \cdot T^{-1} + 39.8858377 - 36.6475723 \cdot T \cdot \ln T - 3.01647572 \cdot 10^{-4} \cdot T^2 + 9.31748907 \cdot 10^{-9} \cdot T^3$
$3400 - 6000 : -142686.075 + 12533841.4 \cdot T^{-1} + 138.179886 - 48.7515496 \cdot T \cdot \ln T + 0.00211768976 \cdot T^2 - 8.28320427 \cdot 10^{-8} \cdot T^3$

SiO_2, gas

$G(Gas, SiO_2) =$
$298.14 - 800 : -318,039.83 + 87,252.9268^{-1} + 12.7262732 \cdot T - 33.977218 \cdot T \cdot \ln T - 0.0236109396 \cdot T^2 + 3.89816307 \cdot 10^{-6} \cdot T^3$
$800 - 2600 : -331,464.671 + 1,432,574.4 \cdot T^{-1} + 184.597402 - 59.850028 \cdot T \cdot \ln T - 8.36931796 \cdot 10^{-4} \cdot T^2 + 5.18207925 \cdot 10^{-8} \cdot T^3$
$2600 - 6000 : -334,879.726 + 2,321,910.8 \cdot T^{-1} + 203.92255 - 62.391808 \cdot T \cdot \ln T + 7.50099152 \cdot 10^{-6} \cdot T^2 - 2.5839338 \cdot 10^{-10} \cdot T^3$

Si

$G(Si,SER) =$
$298.14 - 1687 : -8,162.609 + 137.236859 \cdot T - 22.8317533 \cdot \ln T - 0.001912904 \cdot T^2 - 3.552 \cdot 10^{-9} \cdot T^3 + 176,667 \cdot T^{-1}$
$1687 - 6000 : -9457.642 + 167.281367 \cdot T - 27.196 \cdot T \cdot -4.20369 \cdot 10^{+30} \cdot T^{-9}$

Liquid Si

$G(Si,L) =$
$298.14 - 1687 : +50,696.36 - 30.099439 \cdot T + 2.09307 \cdot 10^{-21} \cdot T^7 + G(Si,SER)$
$1687 - 3600 : +49,828.165 - 29.559069 \cdot T + 4.20369 \cdot 10^{30} - 9 + G(Si,SER)$

C, diamond

$G(C\_Graphite,SER) =$
$298.15 - 6000 : -17,368.441 + 170.73 \cdot T - 24.3 \cdot \ln T - 4.723 \cdot 10^{-4} \cdot T^2 + 2,562,600 \cdot T^{-1} - 2.643 \cdot 10^{8} \cdot T^{-2} + 1.2 \cdot 10^{10} \cdot T^{-3}$

C, diamond

$G(C\_Diamond,SER) =$
$298.15 - 6000 : -16359.441 + 175.61 \cdot T - 24.31 \cdot \ln T - 4.723 \cdot 10^{-4} \cdot T^2 + 2,698,000 \cdot T^3 - 2.61 \cdot 10^{8} \cdot T^{-2} + 1.11 \cdot 10^{10} \cdot T^{-3}$

Liquid Meta

(C, Si)

Gibbs energy for end-members
$G(LM,C) = 298.15 - 6000 : +117374.03 - 24.63 + G(C\_Graphite,SER)$
$G(LM,Si) = 298.14 - 1687 : +50,696.36 - 30.099439 \cdot T + 2.09307 \cdot 10^{-21} \cdot T^7 + G(Si,SER)$
$1687 - 3600 : +49,828.165 - 29.559069 \cdot T + 4.20369 \cdot 10^{30} - 9 + G(Si,SER)$

Mixing parameters

$L_0(LM,C,Si) = 298.15 - 6000 : +25,644.97 - 6.39115 \cdot T$

Diamond

$(C, Si)_P(O, va)_Q$

Gibbs energy for end-members
$G(Diamond,C:O) = 298.15 - 6000 : 0$
$G(Diamond,Si:O) = 298.14 - 1000 : +26519.13 - 25.503038 \cdot T - 11.136 \cdot \ln T - 0.005098888 \cdot T^2 + 6.61846 \cdot 10^{-7} \cdot T^3 - 38365 \cdot T^{-1}$
$1000 - 3300 : +23431.237 + 12.65988 \cdot T - 16.8138 \cdot T \cdot -5.95798 \cdot 10^{-4} \cdot T^2 + 6.781 \cdot 10^{-9} \cdot T^3 + 262905 \cdot T^{-1}$
$3300 - 6000 : +16,013.272 + 31.259625 \cdot T - 18.9536 \cdot T \cdot -4.25243 \cdot 10^{-4} \cdot T^2 + 1.0721 \cdot 10^{-8} \cdot T^3 + 4,383,200 \cdot T^{-1}$
$G(Diamond,C:va) = 298.15 - 6000 : G(C\_Diamond,SER)$
$G(Diamond,Si:va) = 298.15 - 6000 : G(Si,SER)$

(continued)

Table 1 Thermodynamic descriptions as used for the calculation of yttrium silicate coating reactions (continued)

Mixing parameters

L_0(Diamond,Si:O, va) = 298.15 − 6000 : −340, 000 + 85.3 · T

SiC

G(SiC) = 298.15 − 6000 : −88, 583.96 + 271.14622 · T − 41.279456 · T · ln T − 0.00436266 · T^2 + 800, 000 · T^{-1} + 2 · 10^{-7} · T^3

SiO_2, quartz

G(SiO_2, Q) =
298.14 − 540 : −900, 936.64 − 360.892175 · T + 61.1323 · T · ln T − 0.189203605 · T^2 + 4.9509742 · 10^{-5} · T^3 − 854401 · T^{-1}
540 − 770 : −1, 091, 466.54 + 2, 882.67275 · T − 452.1367 · T · ln T + 0.428883845 · T^2 − 9.0917706 · 10^{-5} · T^3 + 12476689 · T^{-1}
770 − 848 : −1563481.44 + 9, 178.58655 · T − 1404.5352 · T · ln T + 1.28404426 · T^2 − 2.35047657 · 10^{-4} · T^3 + 5, 6402, 304 · T^{-1}
848 − 1800 : −928, 732.923 + 356.218325 · T − 58.4292 · T · ln T − 0.00515995 · T^2 − 2.47 · 10^{-10} · T^3 − 95, 113 · T^{-1}
1800 − 2960 : −924, 076.574 + 281.229013 · T − 47.451 · T · ln T − 0.01200315 · T^2 + 6.78127 · 10^{-7} · T^3 + 665, 385 · T^{-1}
2960 − 4000 : −957, 997.4 + 544.992084 · T − 82.709 · T · ln T

SiO_2, cristobalite

G(SiO_2, C) =
298.14 − 373 : −601467.73 − 8140.2255 · T + 1, 399.8908 · T ln T − 2.8579085 · T^2 + 0.0010408145 · T^3 − 13, 144, 016 · T^{-1}
373 − 453 : −1, 498, 711.3 + 13, 075.913 · T − 2178.3561 · T ln T + 3.493609 · T^2 − 0.0010762132 · T^3 + 29, 100, 273 · T^{-1}
453 − 543 : −3, 224, 538.7 + 47, 854.938 · T − 7, 860.2125 · T ln T + 11.817149 · T^2 − 0.0033651832 · T^3 + 1.2750272 · 10^{+8} · T^{-1}
543 − 3300 : −943, 127.51 + 493.26056 · T − 77.5875 · T ln T + 0.003040245 · T^2 − 4.63118 · 10^{-7} · T^3 + 2, 227, 125 · T^{-1}
3300 − 4000 : −973, 891.99 + 587.0506 · T − 87.373 · T ln T

SiO_2, tridymite

G(SiO_2, T) =
298.14 − 388 : −918, 008.73 + 140.55925 · T − 25.1574 · T · ln T − 0.0148714 · T^2 − 2.2791833 · 10^{-5} · T^3 + 66331 · T^{-1}
388 − 433 : −921, 013.31 + 224.53808 · T − 37.8701 · T · −0.02368535 · T^2 − 1.6835 · 10^{-7} · T^3
433 − 900 : −919, 633.42 + 210.51651 · T − 35.605 · T · −0.03049985 · T^2 + 4.6255 · 10^{-6} · T^3 − 162, 026 · T^{-1}
900 − 1668 : −979, 377.7 + 848.3098 · T − 128.434 · T · +0.03387055 · T^2 − 3.786883 · 10^{-6} · T^3 + 7, 070, 800 · T^{-1}
1668 − 3300 : −943, 685.26 + 493.58035 · T − 77.5875 · T · ln T + 0.003040245 · T^2 − 4.63118 · 10^{-7} · T^3 + 2, 227, 125 · T^{-1}
3300 − 4000 : −974, 449.74 + 587.37585 · T − 87.373 · T · ln T

Liquid SiO_2

G(SiO_2, L) =
298.14 − 2980 : −923, 689.98 + 316.24766 · T − 52.17 · T · ln T − 0.012002 · T^2 + 6.78 · 10^{-7} · T^3 + 665, 550 · T^{-1}
2980 − 4000 : −957, 614.21 + 580.01419 · T − 87.428 · T · ln T

Liquid Y

G(Y,L) =
298.14 − 1799 : +3934.121 + 59.921688 · T − 14.8146562 · T · ln T − 0.015623487 · T^2 + 1.442946 · 10^{-6} · T^3 − 140695 · T^{-1}
1799 − 6000 : −13, 337.609 + 258.004539 · T − 43.0952 · T · ln T

Liquid Y_2O3

G(Y_2O_3, L) =
298.15 − 6000 : −1, 821, 322.19 + 243.52552 · T + 2 · G(Y,L) + 1.5 · G(Gas, O_2)

Y_2O_3, H (yttria, hexagonal)

$(Y^{+3})_P(O^{-2}, va^{-2})_Q$

Gibbs energy for end-members

G(Y_2O_3H,Y^{+3} : O^{-2}) = 298.15 − 6000 : −1, 956, 736 + 754.10313 · T − 125.692 · T · ln T − 0.00558 · T^2 + 2344020.5 · T^{-1} − 1.1730556 · 10^{+8} · T^{-2}
G(Y_2O_3H,Y^{+3}:va^{-2}) = 298.15 − 6000 : +340, 026.026 − 107.540058 · T + 2 · G(Y,SER)
G(Y,SER) = 298.14 − 1500 : −7, 347.055 + 117.532124 · T − 23.8685 · T · ln T − 0.003845475 · T^2 + 1.1125 · 10^{-8} · T^3 − 16486 · T^{-1}
1500 − 1799 : −15, 802.62 + 229.831717 · T − 40.2851 · T · ln T + 0.0068095 · T^2 − 1.14182 · 10^{-6} · T^3
1799 − 6000 : −72, 946.216 + 393.885821 · T − 58.2078433 · T · ln T + .002436461 · T^2 − 7.2627 · 10^{-8} · T^3 + 20, 866, 567 · T^{-1}

Y_2O_3, R (yttria, cubic C-type)

$(Y^{+3})_P(O^{-2}, va^{-2})_Q$

(continued)

Table 1 Thermodynamic descriptions as used for the calculation of yttrium silicate coating reactions (continued)

Gibbs energy for end-members

$G(Y_2O_3,R,Y^{+3}:O^{-2}) = 298.15 - 6000 : -1,981,736 + 763.71851 \cdot T - 125.692 \cdot T \cdot \ln T - 0.00558 \cdot T^2 + 2,344,020.5 \cdot T^{-1} - 1.1730556 \cdot 10^{+8} \cdot T^{-2}$

$G(Y_2O_3,R,Y^{+3}:va^{-2}) = 298.15 - 6000 : +340,026.026 - 107.540058 \cdot T + 2 \cdot G(Y,SER)$

Y_2SiO_5

$G(Y_2SiO_5) =$
$298.15 - 6000 : -2,962,274 + 1,057.09397 \cdot T - 181.294814 \cdot T \cdot \ln T - 0.0110113475 \cdot T^2 + 1,803,500.83 \cdot T^{-1}$

$Y_2Si_2O_7$, δ

$G(Y_2Si_2O_7,\delta) =$
$298.15 - 6000 : -3922266.08 + 1588.87798 \cdot T - 264.23561 \cdot T \cdot -0.0129019088 \cdot T^2 + 3559383.17 \cdot T^{-1}$

$Y_2Si_2O_7$, γ

$G(Y_2Si_2O_7,\gamma) =$
$298.15 - 6000 : -3924305 + 1589.97798 \cdot T - 264.23561 \cdot T \cdot -0.0129019088 \cdot T^2 + 3559383.17 \cdot T^{-1}$

$Y_2Si_2O_7$, β

$G(Y_2Si_2O_7,\beta) =$
$298.15 - 6000 : -3926090.28 + 1591.07798 - 264.23561 \cdot T \cdot -0.0129019088 \cdot T^2 + 3559383.17 \cdot T^{-1}$

$Y_2Si_2O_7$, α

$G(Y_2Si_2O_7,\alpha) =$
$298.15 - 6000 : -3927699.58 + 1591.07798 \cdot T - 264.23561 \cdot T \cdot -0.0129019088 \cdot T^2 + 3559383.17 \cdot T^{-1}$

Ionic Liquid

$(Si^{+4}, Y^{+3})_P(O^{-2}, SiO_4^{-4}, va, SiO_2)_Q$

Gibbs energy for end-members

$G(Ionic\_Liq, Si^{+4}:O^{-2}) = 298.15 - 6000 : 2 \cdot G(SiO_2,L) + 2000000$
$G(Ionic\_Liq, Y^{+3}:O^{-2}) = 298.15 - 6000 : 2 \cdot G(Y_2O_3,L)$
$G(Ionic\_Liq, Si + 4 : SiO_4^{-4}) = 298.15 - 6000 : 8 \cdot G(SiO_2,L) + 2000000$
$G(Ionic\_Liq, Y^{+3}:SiO_4^{-4}) = 298.15 - 6000 : 2 \cdot G(Y_2O_3,L) + 3 \cdot G(SiO_2,L) + 54487.7131 - 139.680116 \cdot T$
$G(Ionic\_Liq,Si^{+4}:va) = 298.15 - 6000 : +G(Si,L)$
$G(Ionic\_Liq,Y^{+3}:va) = 298.15 - 6000 : +G(Y,L)$
$G(Ionic\_Liq,SiO_2) = 298.15 - 6000 : G(SiO_2,L)$

Mixing parameters

$L_0(Ionic\_Liq,Si^{+4}:O^{-2},va) = 298.15 - 6000 : -1,482,600 + 14.4 \cdot T$
$L_0(Ionic\_Liq,Y^{+3}:O^{-2},va) = 298.15 - 6000 : +209,819.073 - 118.227607 \cdot T$
$L_0(Ionic\_Liq,Y^{+3}:O^{-2},SiO_4^{-4}) = 298.15 - 6000 : +1,018,615.91 - 560 \cdot T$
$L_0(Ionic\_Liq,Y^{+3}:O^{-2},SiO_2) = 298.15 - 6,000 : +64,275.7706 - 95.015847 \cdot T$
$L_1(Ionic\_Liq,Y^{+3}:O^{-2},SiO_2) = 298.15 - 6,000 : -577,744.591 + 179.543138 \cdot T$
$L_0(Ionic\_Liq,Si^{+4}:SiO_4^{-4},va) = 298.15 - 6,000 : +250 \cdot T$
$L_0(Ionic\_Liq,Y^{+3}:SiO_4^{-4},SiO_2) = 298.15 - 6,000 : 2 \cdot L_0(Ionic\_Liq,Y^{+3}:O^{-2},SiO_2)$
$L_1(Ionic\_Liq,Y^{+3}:SiO_4^{-4},SiO_2) = 298.15 - 6000 : 2 \cdot L_1(Ionic\_Liq,Y^{+3}:O^{-2},SiO_2)$
$L_0(Ionic\_Liq,Si^{+4},Y^{+3}:va) = 298.15 - 60000 : -212656.12 + 25.83471 \cdot T$
$L_1(Ionic\_Liq,Si^{+4},Y^{+3}:va) = 298.15 - 60000 : +13977.08 - 31.08941 \cdot T$
$L_2(Ionic\_Liq,Si^{+4},Y^{+3}:va) = 298.15 - 60000 : +62049.23 - 50.31476 \cdot T$
$L_0(Ionic\_Liq,Si^{+4}:va,SiO_2) = 298.15 - 6000 : +250 \cdot T$

must equal the combined flux of CO and SiO species away from the SiC surface. This is the mass-balance condition.

Wagner shows[25] that in the viscous gas flow regime, the flux J of a species diffusing through a gaseous boundary layer is given by

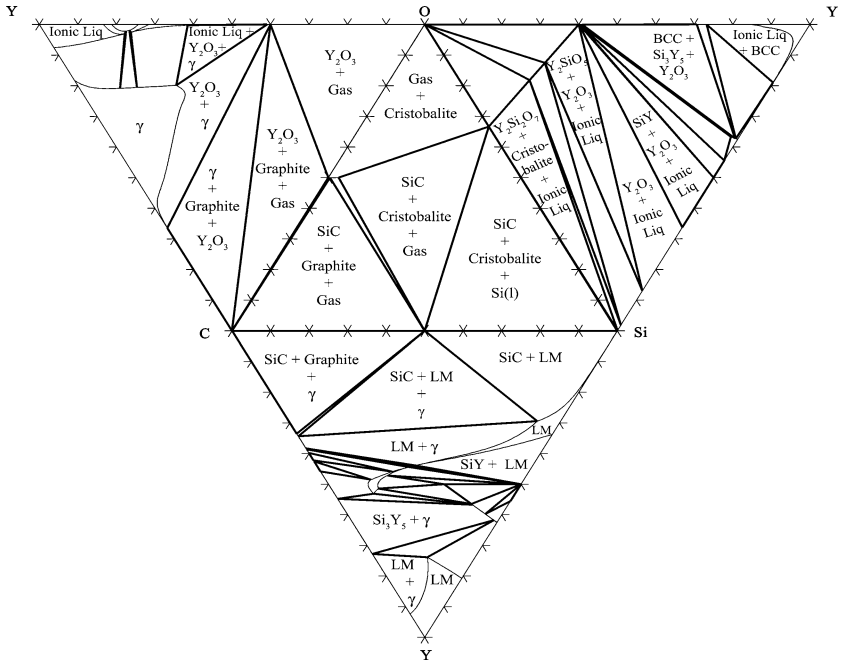

Fig. 1 Calculated isothermal sections of ternary subsystems for the Y-Si-C-O system at 1650 °C

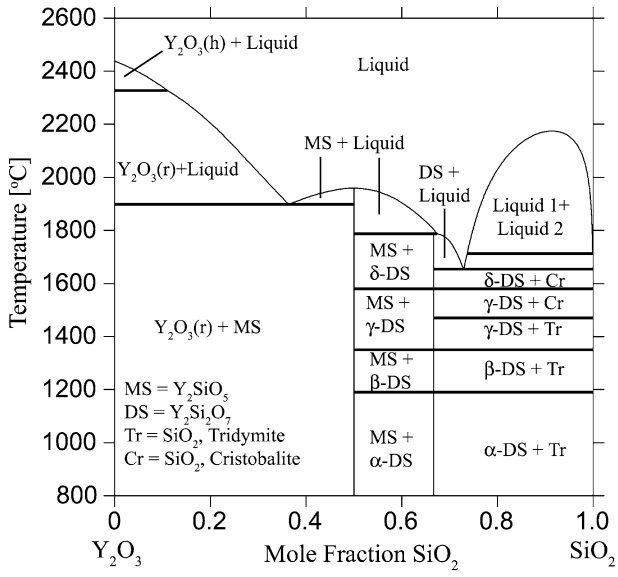

Fig. 2 The calculated pseudo-binary Y_2O_3-SiO_2 phase diagram

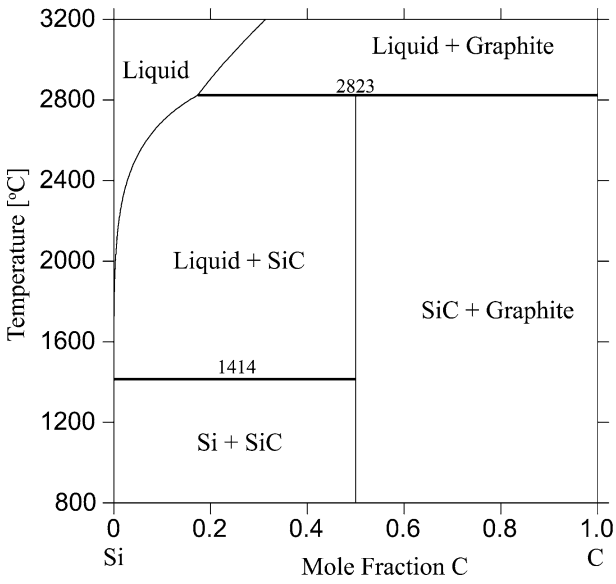

Fig. 3 The calculated binary Si-C phase diagram

$$J_i = \frac{D_i}{\delta_i}\frac{p_i^s - p_i^b}{RT} \qquad \text{(Eq 2)}$$

where the subscript i identifies the gas species, D is the diffusion coefficient, δ is the boundary layer thickness, p^s is the partial pressure at the surface, and p^b is the partial pressure in the bulk gas. p^b is negligible for CO and SiO as it is assumed that there is no CO and SiO in the bulk gas and p^s is negligible for oxygen because it is fully consumed at the SiC surface. The mass-balance conditions according to Eq 1 can be expressed as:

$$J_{SiO} = J_{CO} = -J_{O_2} \qquad \text{(Eq 3)}$$

where the negative sign is used because oxygen diffuses in a direction opposite to that of SiO and CO. Wagner[25] indicates that the ratio of the boundary layer thicknesses of species i and j can be approximated by:

$$\delta_i/\delta_j \approx \sqrt{(D_i/D_j)} \qquad \text{(Eq 4)}$$

Since the diffusivity of a gas is inversely proportional to its molecular weight, substituting (2) into (3) and using

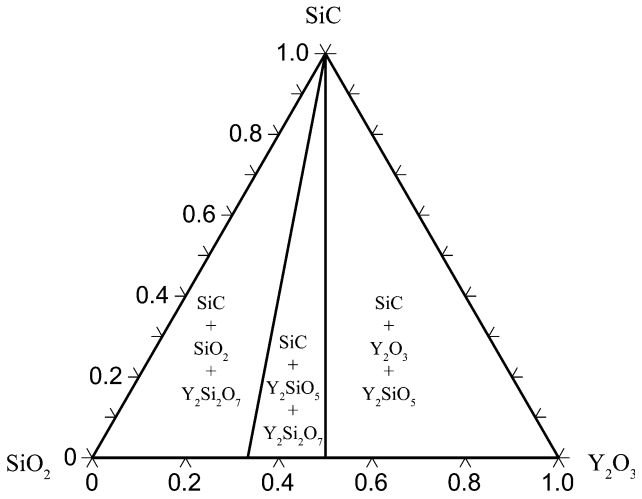

Fig. 4 The calculated pseudo-ternary isotherm SiO_2-Y_2O_3-SiC subsystem of the Y-Si-C-O system at 1650 °C.

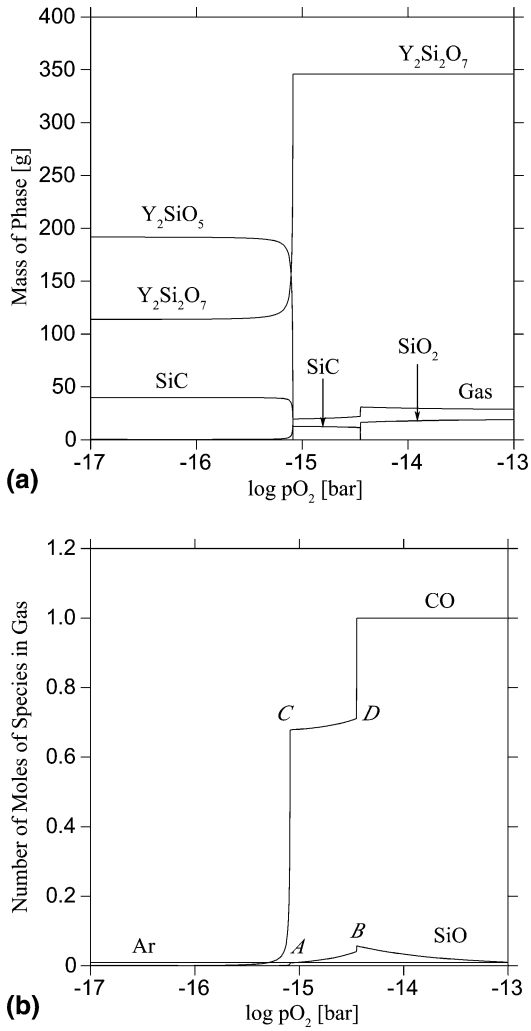

Fig. 5 Thermodynamic simulation of the interface reactions of Y_2SiO_5 and $Y_2Si_2O_7$ with SiC at 1650 °C: (a) phase fraction diagram; (b) related formation of gas species

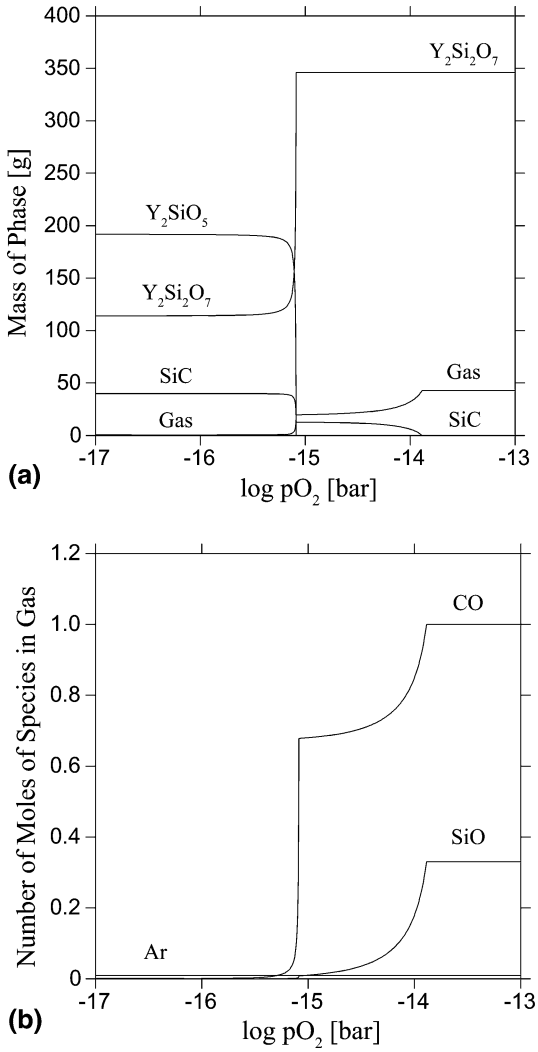

Fig. 6 Thermodynamic simulation of interface reactions of Y_2SiO_5 and $Y_2Si_2O_7$ with SiC at 1650 °C. SiO_2 is suspended; (a) phase fraction diagram; (b) related formation of gas species

(4), one can generate three dependent conditions, all of which must be satisfied during the active oxidation of SiC. These are:

$$\frac{p_{CO}}{p_{SiO}} = \left(\frac{D_{SiO}}{D_{CO}}\right)^{1/2} = \left(\frac{M_{CO}}{M_{SiO}}\right)^{1/2} = 0.80 \qquad \text{(Eq 5)}$$

$$\frac{p_{SiO}}{p_{O_2}} = \left(\frac{D_{O_2}}{D_{SiO}}\right)^{1/2} = \left(\frac{M_{SiO}}{M_{O_2}}\right)^{1/2} = 1.17 \qquad \text{(Eq 6)}$$

$$\frac{p_{CO}}{p_{O_2}} = \left(\frac{D_{O_2}}{D_{CO}}\right)^{1/2} = \left(\frac{M_{CO}}{M_{O_2}}\right)^{1/2} = 0.94 \qquad \text{(Eq 7)}$$

Heuer and Lou[24] showed that the so-called volatility diagrams (isothermal plots showing the partial pressure of major gas species in equilibrium with condensed phases in

the system) are useful to the study of such type of SiC oxidation. In the Si-C-O system, three gas species, SiO_x (x can be 0 or any integer greater than 0 and identifies Si-containing gas species, e.g., Si, SiO, SiO_2), CO, and oxygen are in equilibrium with the condensed phases and the complete volatility diagram for the Si-C-O system is a three-dimensional construction. Heuer and Lou[24], in determining the active to passive transition for SiC by using volatility diagrams, show a volatility diagram for the Si-C-O system calculated at a fixed CO pressure. Narushima et al.[26] also calculate at a fixed CO pressure, although they do not indicate what that pressure is. However, according to Eq 1, as the supply of oxygen to the SiC surface changes, the equilibrium pressure of CO at the surface must necessarily change. Therefore, calculations using a fixed CO pressure at the SiC surface are not in full agreement with the active oxidation model. Further, Heuer and Lou, in using the Wagner model to construct mass-balance conditions for the active oxidation of SiC, chose to ignore the different diffusivities of O_2, SiO, and CO. Their mass-balance conditions are $p_{CO} = p_{SiO} = p_{O_2}$. For a refinement of this approach, Eq 5–7 considering the diffusivities of the gaseous species should be taken into account.

Figure 7 shows the volatility diagram for SiC at 1650 °C with the mass-balance condition of Eq 5 imposed as a constraint. It was calculated by using Gibbs free energy minimization algorithms. Heuer et al.[24] constructed volatility diagrams by considering the thermochemistry for all possible reaction equations in the system. By using advanced software there is no more need to list all possible reaction equations for the system (and easily miss one). Figure 7 can be thought of as a calculation on the plane $p_{CO} = 0.8p_{SiO}$ in the three-dimensional Si-C-O volatility diagram, represented as plane ABCD in Fig. 8. The dashed line in Fig. 7, analogous to the isomolar line of Heuer, represents the conditions of Eq 6. It intersects the volatility diagram at point B. Figure 8 shows the isomolar line in the three-dimensional Si-C-O volatility diagram as line AC. It is the intersection of plane ABCD generated by Eq 5 with plane AECF from Eq 6. It also maps the actual oxygen, SiO, and CO pressure development at the SiC interface during active oxidation. The intersection of this line with the volatility diagram at point B gives the lower limit of the active to passive transition for SiC. At this point, SiO_2 smoke forms away from the SiC surface. At 1650 °C, the oxygen partial pressure at the lower limit is $10^{-5.71}$ bar. From Eq 6 and 7 it follows that the CO- and SiO-partial pressures at the lower limit are $10^{-5.74}$ and $10^{-5.64}$ bar, respectively.

Heuer and Lou[24], in accordance with the Wagner model, state that the upper limit of the active to passive transition is determined by the partial pressure of SiO at the SiC interface. If the SiO pressure is less than that required for equilibrium between SiC and SiO_2, p^{eq}_{SiO}, then active oxidation of SiC will persist. The passivating SiO_2 layer will only form when the SiO pressure at the SiC surface is greater than p^{eq}_{SiO}. In Fig. 7, the equilibrium partial pressure of SiO occurs at point A and has a value of $10^{-0.9}$ bar. This corresponds to a CO pressure at the equilibrium, p^{eq}_{CO}, of $10^{-1.0}$ bar. At point D, the oxygen pressure of $10^{-1.0}$ bar is sufficient to generate p^{eq}_{SiO} and p^{eq}_{CO} and the SiO_2 layer should form.

Opila and Jacobson[27,28] also treat the diffusion of oxygen, SiO, and CO through a gaseous boundary layer during the active oxidation of SiC. However, the flux of CO determines equilibrium between SiC and SiO_2. Heuer and Lou[24] calculate volatility diagrams at different fixed CO pressures to show the dependence of the upper limit on CO pressure. The treatment presented here is different to that of Opila and Jacobson[28] and Heuer and Lou[24]. Since the pressures of SiO and CO are constrained by the mass-balance condition of Eq 5, both species are equally important in

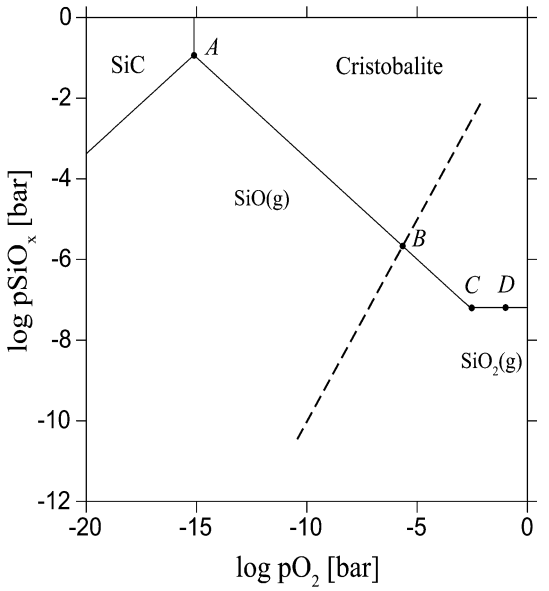

Fig. 7 Volatility diagram for the Si-C-O system at 1650 °C. Calculations were performed for a closed system with the constraint that $p_{CO} = 0.8\ p_{SiO}$ to simulate the mass-balance conditions. At point C, the major Si-containing gas species changes from SiO to SiO_2.

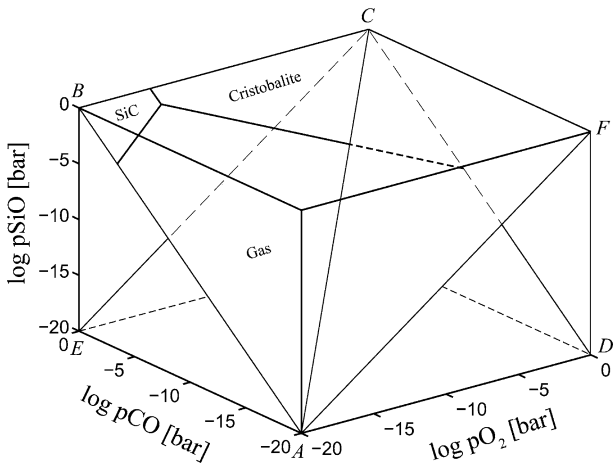

Fig. 8 Three dimensional representation of the mass-balance conditions for the active oxidation of SiC. Equation 5 in text is shown as plane ABCD and Eq 6 in text is shown as plane AECF. The volatility diagram for the Si-C-O system at 1650 °C calculated with the mass-balance condition of Eq 5 is also shown.

determining equilibrium between SiC and SiO_2. Rocabois et al.[29] also analyze the Si-C-O system but do not investigate the active to passive transition of SiC. It has to be emphasized that for the conditions described in this work, CVD-SiC is only directly exposed to gas phase when cracks, open porosity or blisters in the protective yttrium silicate layer exist. Therefore, active/passive oxidation may only occur with coating defects.

3.2 Potential Diagrams in the Y-Si-C-O System

As shown by the calculations[12] the main gas species formed from coating-substrate reactions are CO and SiO. The partial pressures of these gaseous species were chosen to represent the isothermal phase compatibilities of condensed phases in the coating-substrate system (potential diagrams). Figure 9 shows the potential phase diagrams at 1650 °C for the three different possible coating system compositions. Each line in the potential phase diagram indicates four phase equilibria. The points of intersection of these lines represent five-phase equilibria. For all coating compositions, CO is the more dominant species in the gas phase with the highest partial pressure. The oxygen partial pressure is negligible (about 10^{-15} bar) in comparison to the CO- and SiO-partial pressures. In Fig. 9(a), the silicate coating contains Y_2O_3 and Y_2SiO_5. The left-most triangular region represents the three phase equilibrium of gas phase, SiC and Y_2O_3. At 1650 °C, the five-phase equilibrium point (Gas + SiC + Graphite + Y_2O_3 + Y_2SiO_5) occurs at a CO-partial pressure of 0.0487 bar. In Fig. 9(b), coating composition is based on Y_2SiO_5 and $Y_2Si_2O_7$. The left-most triangular region shows the three phase equilibria of gas phase, SiC, and Y_2SiO_5 with the five-phase equilibrium (Gas + SiC + Graphite + $Y_2Si_2O_7$ + Y_2SiO_5) occurring at 1.2 bar CO-partial pressure. Figure 9(c) shows the phase stabilities for $Y_2Si_2O_7$ and SiO_2 (cristobalite). The left-most triangular region shows the equilibrium between gas phase, SiC and cristobalite. Here at the five-phase equilibrium (Gas + SiC + Graphite + Cristobalite + $Y_2Si_2O_7$) the CO-partial pressure is 3.68 bar. In all coatings, the five-phase equilibria represent the maximum possible CO-partial pressure for the corresponding coating system.

Figure 10 shows the dependence of the CO-partial pressure at the five-phase equilibrium point on temperature for the three coating compositions. For example, the temperature dependent partial pressure of carbon monoxide in equilibrium with the four phases Graphite + SiC + Y_2SiO_5 + $Y_2Si_2O_7$ is

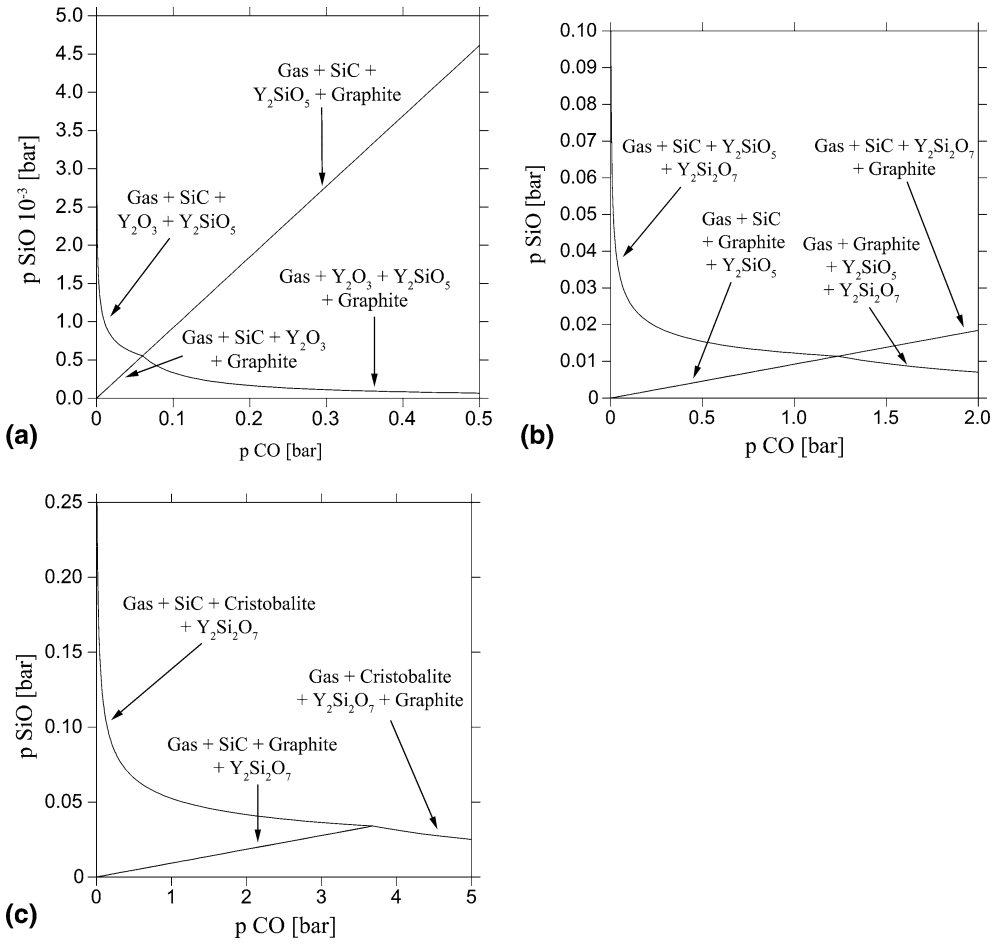

Fig. 9 Volatility diagrams at 1650 °C for three possible coating compositions; (a) coating composition based on Y_2O_3 and Y_2SiO_5; (b) coating composition based on Y_2SiO_5 and $Y_2Si_2O_7$; (c) coating composition based on $Y_2Si_2O_7$ and SiO_2

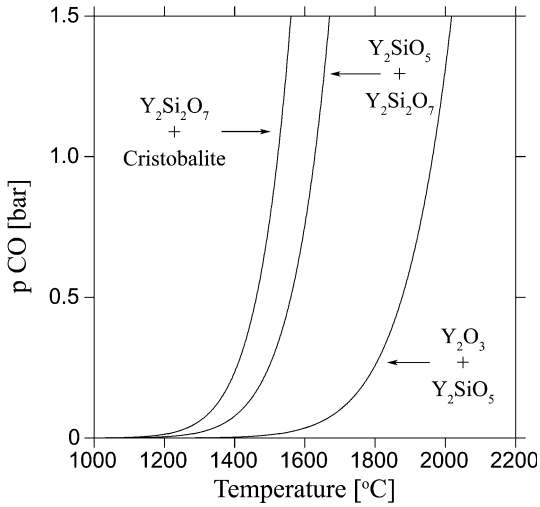

Fig. 10 CO-partial pressures for the five-phase equilibria as a function of temperature for three coating compositions

indicated. It significantly increases at temperatures higher than 1300 °C. Additionally, the CO-partial pressure developments for other coating compositions as discussed before are indicated: Graphite + SiC + $Y_2Si_2O_7$ + SiO_2 and Graphite + SiC + Y_2O_3 + Y_2SiO_5, respectively. Obviously, coatings based on combinations of monosilicate and disilicate and disilicate and cristobalite produce significant CO-partial pressures at much lower temperatures than coatings based on yttria and monosilicate. The CO-partial pressure for yttria (Y_2O_3) containing coatings significantly increases only at temperatures above 1500 °C. However, the thermal expansion mismatch of Y_2O_3 with the other phases prevents the commercial use of such a coating composition.

Note that these calculations describe unrestricted reactions between the system components and gas species. Results of experiments with powder mixtures of SiC and Y_2SiO_5 are in accordance with calculated results.[12] However, in a multilayer coating, direct contact between all system components and gas species occur only at the interfaces. Nevertheless, the results strongly indicate that gas phase production resulting from coating reactions lead to blister formation.

4. Conclusion

A complete thermodynamic equilibrium and mass-balance analysis of environmental barrier coatings for C/C-SiC ceramic matrix composites based on an outer yttrium silicate layer and an inner SiC layer was presented. The determination of the specific oxygen partial pressure, at which the active oxidation of the inner SiC-layer ceases and the passivating SiO_2 layer forms, was discussed. In this case, mass-balance considerations must be taken into account. According to the calculations, active oxidation of SiC should cease only when the oxygen partial pressure at the SiC surface is 10^{-1} bar. Volatility diagrams for three yttrium silicate coating compositions were also presented. These indicate that coatings based on Y_2O_3 and Y_2SiO_5 generate the lowest partial pressure of gas species at the interface with SiC.

References

1. J. Ihle, M. Herrmann, and J. Adler, Phase Formation in Porous Liquid Phase Sintered Silicon Carbide: Part II: Interaction between Y_2O_3 and SiC, *J. Euro. Ceram. Soc.*, 2005, **25**, p 997-1003
2. Y. Ogura, M. Kondo, and T. Morimoto, Y_2SiO_5 as Oxidation Resistant Coating for C/C Composites, *Proc. 10th Int. Conf. on Composite Materials (ICCM-10)*, 1995 (Whistler, B.C., Canada IV), p 767-774
3. J.D. Webster, M.E. Westwood, F.H. Hayes, R. Taylor, A. Duran, M. Aparicio, K. Rebstock, and W.D. Vogel, Oxidation Protection Coatings for C/SiC Based on Y_2SiO_5, *Key Eng. Mater.*, 1997, **132–136**, p 1641-1644
4. J.D. Webster, M.E. Westwood, F.H. Hayes, R.J. Day, R. Taylor, A. Duran, M. Aparicio, K. Rebstock, and W.D. Vogel, Oxidation Protection Coatings for C/SiC Based on Yttrium Silicate, *J. Euro. Ceram. Soc*, 1998, **18**, p 2345-2350
5. M. Aparicio and A. Duran, Yttrium Silicate Coatings for Oxidation Protection of Carbon-Silicon Carbide Composites, *J. Am. Ceram. Soc.*, 2000, **83**(6), p 1351-1355
6. Y. Ogura, M. Kondo, T. Morimoto, A. Notomi, and T. Sekigawa, Oxidation Behavior of Y_2SiO_5/SiC Coatings in Low Pressures of Oxygen, *J. Japan Inst. Metals*, 2001, **65**(1), p 13-20
7. J.F. Huang, X.R. Zeng, H.J. Li, X.B. Xiong, Y.W. Fu, and M. Huang, SiC/Yttrium Silicate Multi-layer Coating for Oxidation Protection of Carbon/Carbon Composites, *J. Mater. Sci.*, 2004, **39**, p 7383-7385
8. T. Ullmann, M. Schmücker, H. Hald, R. Henne, and H. Schneider, Oxidation Protection of C/SiC Composites Based on Plasma-sprayed Y-Silicates, *Proc. 8th Int. Symp. Mater. in Space Environm. & 5th Int. Conf. Protection Mater. and Structures from LEO Space Environm.*, 5-9 June 2000, Arcachon, France on CD, 2000
9. T. Laux, T. Ullmann, M. Auweter-Kurtz, H. Hald, and A. Kurz, Investigations of Thermal Protection Materials along an X-38 Re-entry Trajectory by Plasma Wind Tunnel Simulations, *Proc. 2nd Int. Symp. Atmospheric Reentry Vehicles and Systems*, 26–29 March 2001, Arcachon, France on CD, 2001
10. M. Aparicio, R. Moreno, and A. Duran, Colloidal Stability and Sintering of Yttria-Silica and Yttria-Silica-Alumina Aqueous Suspensions, *J. Eur. Ceram. Soc.*, 1999, **19**, p 1717-1724
11. M. Aparicio and A. Durán, Preparation and Characterization of $50SiO_2$-$50Y_2O_3$ Sol-Gel Coatings on Glass and SiC(C/SiC) Composites, *Ceram. Int.*, 2005, **31**, p 631-634
12. H.J. Seifert, S. Wagner, O. Fabrichnaya, H.L. Lukas, F. Aldinger, T. Ullmann, M. Schmücker, and H. Schneider, Yttrium Silicate Coatings on Chemical Vapor Deposition-SiC-Precoated C/C-SiC: Thermodynamic Assessment and High Temperature Investigation, *J. Am. Ceram. Soc.*, 2005, **88**, p 424-430
13. N. Saunders and P. Miodownik, CALPHAD (Calculation of Phase Diagrams): A Comprehensive Guide, in *Materials Series Vol. 1*., R.W. Cahn, ed. Oxford, Pergamon, 1998
14. Scientific Group Thermodata Europe (SGTE), Grenoble Campus, 1001 Avenue Centrale, BP66, F-38402 Saint Martin d'Heres, France, http://www.sgte.org

15. J. Gröbner, Konstitutionsberechnungen im System Y-Al-Si-C-O, PhD Thesis, University of Stuttgart, 1994
16. V. Swamy, H.J. Seifert, and F. Aldinger, Thermodynamic Properties of Y_2O_3 Phases and the Yttrium-Oxygen Phase Diagram, *J. Alloys Comp.*, 1998, **269**, p 201-207
17. B. Hallstedt, Thermodynamic Assessment of the Silicon-Oxygen System, *CALPHAD*, 1992, **16**(1), p 53-61
18. O. Fabrichnaya, H.J. Seifert, R. Weiland, T. Ludwig, F. Aldinger, and A. Navrotsky, Phase Equilibria and Thermodynamics in the Y_2O_3-Al_2O_3-SiO_2 System, *Z. Metallkd.*, 2001, **92**, p 1083-1097
19. H.L. Lukas and S.G. Fries, Demonstration of the Use of BINGSS with the Mg-Zn System as Example, *J. Phase Equilib.*, 1992, **13**(5), p 532-541
20. J.-O. Andersson, T. Helander, L. Höglund, P. Shi, and B. Sundman, Thermo-Calc and Dictra, Computational Tools for Materials Science, *CALPHAD*, 2002, **26**(2), p 273-312
21. W.L. Vaughn and H.G. Maahs, Active-to-Passive Transition in the Oxidation of Silicon Carbide and Silicon Nitride in Air, *J. Am. Ceram. Soc.*, 1990, **73**(6), p 1540-1543
22. T. Goto, T. Narushima, Y. Iguchi, and T. Hirai, Active to Passive Transition in the High-Temperature Oxidation of CVD SiC and Si_3N_4, in *Corrosion of Advanced Ceramics*, K.G. Nickel, ed. Kluwer Academic Publishers, Netherlands, 1994, pp. 165-176
23. T. Goto, H. Homma, and T. Hirai, Effect of Oxygen Partial Pressure on the High-Temperature Oxidation of CVD SiC, *Corrosion Sci.*, 2002, **44**, p 359-370
24. A.H. Heuer and V.L.K. Lou, Volatility Diagrams for Silica, Silicon Nitride, and Silicon Carbide and their Application to High-Temperature Decomposition and Oxidation, *J. Am. Ceram. Soc.*, 1990, **73**(10), p 2789-2803
25. C. Wagner, Passivity during the Oxidation of Silicon at Elevated Temperatures, *J. Appl. Phys.*, 1958, **29**(9), p 1295-1297
26. T. Narushima, T. Goto, T. Hirai, and Y. Iguchi, High-Temperature Oxidation of Silicon Carbide and Silicon Nitride, *Mater. Trans. JIM*, 1997, **38**(10), p 821-835
27. E.J. Opila and N.S. Jacobson, SiO(g) Formation from SiC in Mixed Oxidizing-Reducing Gases, *Oxid. Met.*, 1995, **44**(5/6), p 527-544
28. E.J. Opila and N.S. Jacobson, Corrosion of Ceramic Materials, in *Materials Science and Technology Corrosion and Environmental Degradation Vol. II*, R.W. Cahn, P. Haasen and E.J. Kramer, eds. Wiley-Vch, Weinheim, 2000, pp. 327-388
29. P. Rocabois, C. Chatillon, and C. Bernard, High-Temperature Analysis of the Thermal Degradation of Silicon-Based Materials. II: Ternary Si-C-O, Si-N-O, and Si-C-N compounds, *High Temp. High Press.*, 1999, **31**, p 433-454